NANO LETTERS

2006
Vol. 6, No. 4
848−853

Nano Fountain Pen Manufacture of Polymer Lenses for Nano-biochip Applications

Mordechai Sokuler and Levi A. Gheber*

Department of Biotechnology Engineering, Ben-Gurion University of the Negev, P.O. Box 653, Beer-Sheva 84105, Israel

Received February 11, 2006; Revised Manuscript Received March 6, 2006

ABSTRACT

Polymer microlenses have been manufactured by delivering droplets of a monomer mixture to a glass substrate using a nano fountain pen (NFP). Subsequent UV polymerization yielded microlenses with optical properties that were controlled by varying the deposition time of the monomer solution. Using this approach, it is possible to strategically place single microlenses at predefined positions with very high accuracy, an ability which may prove very useful for nano-biochip applications, as demonstrated.

Microlenses have wide applications in consumer products, such as flat panel displays, photocopiers, laser printers, etc. Typical fabrication methods include ink-jet processes,[1,2] use of mesh-shaped masks,[3] lithography, electroforming and plastic molding,[4] direct laser fabrication,[5] and others. Microlenses are typically manufactured as large, dense, ordered arrays, suitable for the optoelectronic applications described.

Another set of applications could greatly benefit from single, precisely positioned microlenses. Nano-biochips (arrays of sub-micrometer dots of biological molecules), an area drawing considerable recent interest,[6−25] could profit in the future from strategically placed individual microlenses, with tailored optical characteristics, small size, and very precise positioning. Miniaturization of biochips is expected to tremendously increase their portability, thus expanding the use of these arrayed biosensors to point-of-care clinical testing, environmental monitoring, etc. The expected decrease in fluorescence signal, due to reduction in the number of biological molecules, and the need to integrate the optical reading systems with the biochip suggest that such optical elements should help to overcome some of the expected challenges. However, the existing methods of microlens manufacture are not suitable for this kind of application.

We present here a method of manufacturing polymer microlenses using a scanning probe microscopy (SPM) technique. A cantilevered nanopipet, mounted as the probe of an atomic force microscope, is used to deliver minute volumes of monomer solution in selected positions, followed by UV-assisted polymerization. This results in spherical polymer microlenses that can be characterized with atomic force microscopy (AFM) for their geometrical properties and with near-field scanning optical microscopy (NSOM) for their optical properties.

Using this approach, we are able to directly "write" microlenses with diameters of 4 μm and up (smaller diameters are easily achievable, however they are not optically useful).

The nano fountain pen (NFP) uses hollow glass or quartz capillaries heat-drawn to a tapered tip with an aperture of a few hundred nanometers.[26] When prepolymerization solution is loaded in such nanopipets, it is drawn to the end of the tapered tip by capillary forces; however the solution will flow out only upon contact with the surface. The nanopipet is mounted as the probe of an atomic force microscope and can be controllably directed to very precise locations on a surface, using the regular control of an atomic force microscope probe.

Lens deposition, AFM characterization, and optical NSOM characterization were performed in ambient conditions, all with the same system: a Nanonics NSOM/AFM 100 system (Nanonics, Jerusalem, Israel) with a flat scanner, which allows two coaxial optical microscopes to examine the sample simultaneously, from top and bottom. NFP probes were cantilevered nanopipets, 600 nm aperture diameter, Cr/Au covered cantilevers of 500−600 μm length (Nanonics, Jerusalem, Israel). Atomic force microscope probes were "Ultrasharp" gold-covered silicon contact cantilevers (Mikromasch, CSC12/CR-Au/15). Cantilevered NSOM probes had 50−100 nm apertures, with Cr/Au covered cantilevers of 500−600 μm and were made of single mode (488 nm) optical fiber (Nanonics, Jerusalem, Israel). Droplets of monomer where placed on glass cover-slips (16 mm diam-

* Corresponding author. E-mail: glevi@bgumail.bgu.ac.il.

10.1021/nl060323e CCC: $33.50
Published on Web 03/18/2006

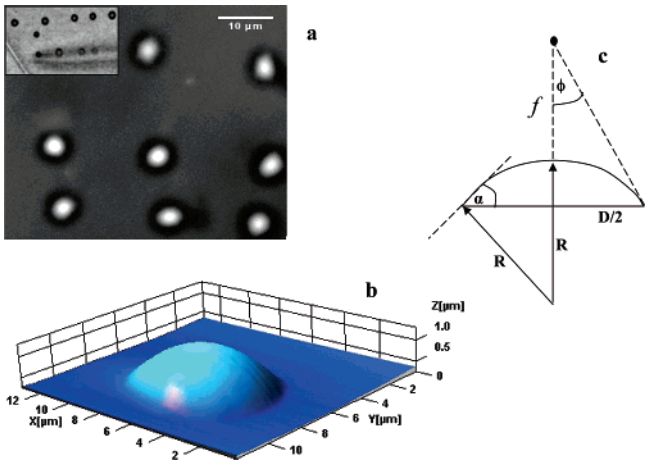

Figure 1. (a) An array of microlenses, illuminated with white light from behind. The inset shows the process of manufacture: some drops of various sizes and the out-of-focus nanopipet, about to print one more microlens. (b) 3D representation of one lens, as characterized with AFM. (c) Definition of the symbols used in the equations: R is the radius of curvature of the lens, D is the diameter of the lens, α is the contact angle, ϕ is half the angle of the light cone available to the lens from its focal point, and f is the lens focal length.

eter; Marienfeld, Germany). A video showing the writing process is provided as Supporting Information.

The monomer mixture used is 20 μL of trimethylolpropane trimethacrylate (TRIM) (Sigma), 30 μL of 2-methoxylethyl ether, anhydrous 99.5% (diglyme) (Aldrich), and 1 mg of 2,2-dimethoxy-2-phenylacetophenone (DPAP/DMPA) (Fluka) used as initiator. Following deposition, drops were polymerized in argon atmosphere under 6 W irradiation of wavelength 254 nm from a Vilber Lourmat UV lamp, at a distance of 3 cm from the light source, for 5 min.

AFM characterization of the polymerized droplets reveals that they form smooth spherical caps, with an root mean square roughness of 1.6 nm. An example of a group of microlenses thus manufactured is presented in Figure 1a and its topography obtained with AFM is shown in Figure 1b.

To investigate the dependence of lens geometry on writing parameters, lenses were deposited by contacting the pipet with the surface for various durations between 1 and 20 s. Following polymerization, the resulting microlenses were characterized using AFM. From the AFM images, we extracted the diameter, radius of curvature, contact angle, and volume, for lenses manufactured with various deposition times.

Diameters of lenses ranged between 4 and 9 μm for deposition time ranging between 1 and 20 s, respectively. The dependence of the lens diameter on deposition time is plotted in Figure 2 a. Error bars represent the standard deviation of the values obtained using three different pipets of the same nominal aperture and four different sets of lenses printed on three different surfaces.

The lens diameter increases with deposition time in a nonlinear fashion, approaching an asymptotic value for long deposition times. This final value represents the equilibrium between the various forces acting on the liquid, such as wetting of the surface, capillary forces pushing the liquid out of the pipet, surface tension of the forming drop, atmospheric pressure, and gravity. At any rate, this dependence on deposition time provides a tool for manipulating the optical properties of the lenses, as shown below.

Equation 1 defines the relationship between the radius of curvature and the diameter of the lens, where R is the radius of curvature, D is the diameter of the droplet, and α is the contact angle, as defined in Figure 1c

$$R = \frac{D}{2 \sin \alpha} \tag{1}$$

Since the contact angle is fixed for a given liquid wetting a surface, the relationship between the diameter and radius of curvature of the polymerized drops is fixed by the contact angle.

The contact angle, radius of curvature and diameter of the droplet can be directly measured from the AFM images, to verify that these relationships hold in reality. In the example shown in Figure 2b, $R = 9$ μm, $\alpha = 16°$, and $D = 5.6$ μm, as directly measured from the AFM data; the diameter predicted by eq 1 is 5.24 μm, for the measured radius of curvature and contact angle, showing that the surface of the lens is indeed spherical. The inset of Figure 2b shows the difference between the fitted curve and the experimental

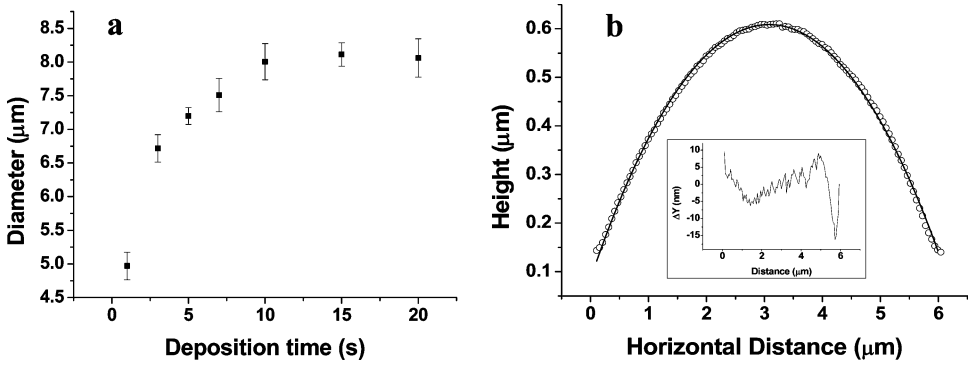

Figure 2. (a) Dependence of lens diameter on the deposition time. (b) The radius of curvature is directly determined from the diameter and contact angle. The continuous line is a fit to the experimental points (circles). The inset shows the difference between the fitted curve and the experimental points, with a peak-to-peak value of 25 nm and a root mean square value of 4.77 nm.

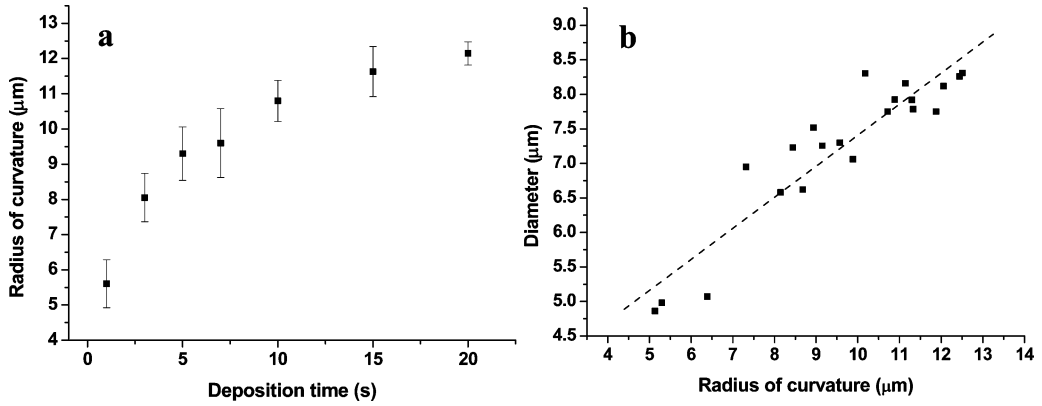

Figure 3. (a) Radius of curvature as a function of deposition time of the monomer solution. (b) Plot of the lens diameter versus the lens radius of curvature. The dependence is expected to be linear (see eq 1), with a slope determined by the contact angle. The dashed line is a linear fit to the measured data, yielding an average contact angle of ∼13°.

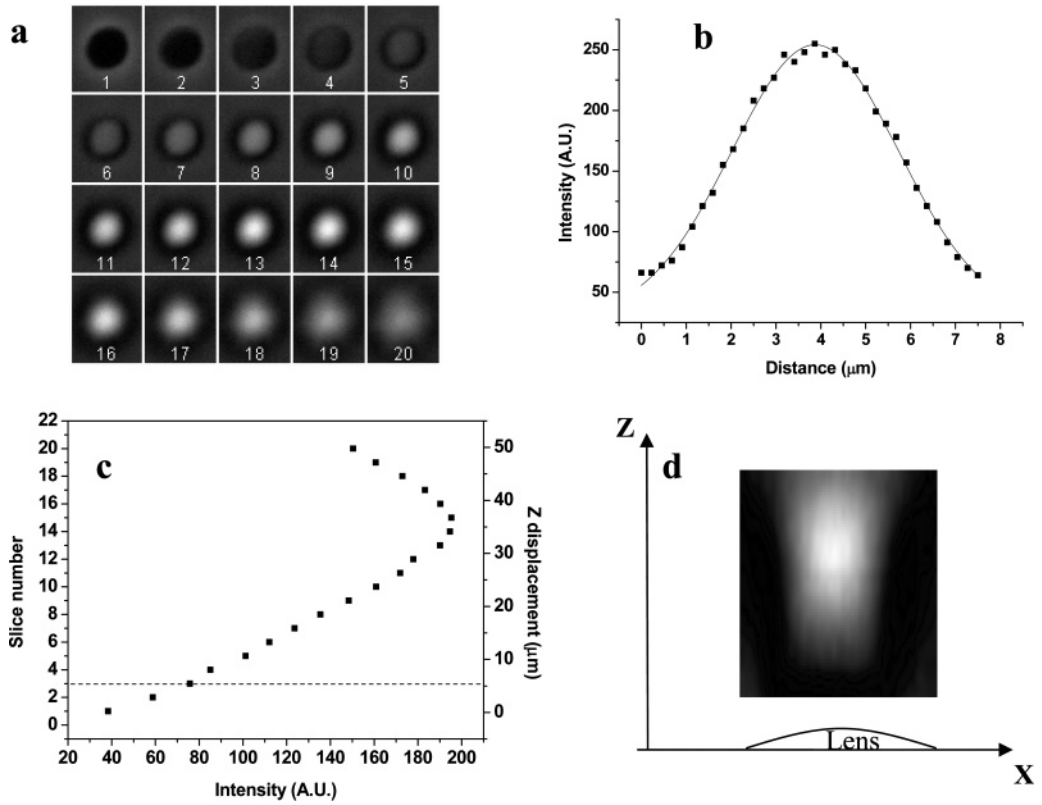

Figure 4. (a) A series of images of light focused through one microlens, starting below the plane of the lens (slice 1), through the focal plane (slices 14, 15), and above it (slices 16−20). (b) The intensity profile along the *X* axis (in the focal plane). The continuous line is a fitted Gaussian with a full width at $1/\sqrt{e}$ maximum of 3.7 μm. (c) The intensity profile along the *Z* axis (optical axis of the lens). The dashed line represents the plane of the lens. The focal plane is at $Z = 35$ μm, where the light intensity is maximal. (d) A stack formed of the slices 1−20 (in Figure 4a) was sectioned along the $X-Z$ plane, to obtain the light intensity distribution in this plane.

points. The peak-to-peak difference is 25 nm (mainly contributed by deviations at the point of contact of the lens with the surface), and the root mean square difference is 4.7 nm. But since the diameter can be controlled by the deposition time, as shown in Figure 2a, it follows that the radius of curvature can be controlled by the deposition time too. To show this, we present the measured radius of curvature as a function of deposition time in Figure 3a. Error bars represent the standard deviation of the values obtained using three different pipets of the same nominal aperture and four different sets of lenses printed on three different surfaces.

It can be seen that the radius of curvature changes nonlinearly with time, as expected, and in fact should be proportional to the lens diameter (see eq 1). A plot of the diameter versus radius of curvature should be linear, with a slope equal to twice the sine of the contact angle, which is assumed to be constant. Such a plot is presented in Figure 3b, which shows indeed a linear behavior, and the linear fit yields an average contact angle of 13°.

Having established the geometrical relationship between the various lens parameters, we proceed to discuss the implications of controlling their optical properties. Given the

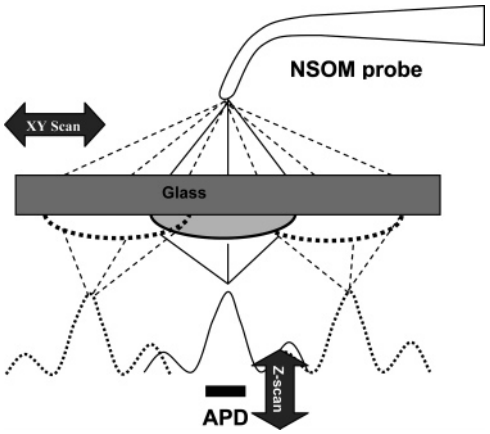

Figure 5. NSOM characterization setup. A NSOM probe is positioned in the far field, serving as a point source of light. The glass substrate with lenses deposited on it was scanned in the *x* and *y* directions with the NSOM scanner, and the intensity of light projected by the lens was recorded with an APD, as a function of the coordinates of the sample. The plane of the APD is changed and the *x*,*y* scan is repeated, thus obtaining a series of intensity maps.

radius of curvature, the focal length of a plano-convex (thin) lens is given by

$$f = \frac{R}{n_{\text{lens}} - 1} = \frac{D}{2(n_{\text{lens}} - 1)\sin\alpha} \qquad (2)$$

where n_{lens} is the refractive index of the polymer, and the second equality in eq 2 makes use of the relationship described by eq 1. Thus, controlling the time of deposition determines the diameter of the lens, its radius of curvature (since the contact angle is constant), and, as a result, the focal length. A rough estimation, taking an index of refraction of $n = 1.55$ (an average refractive index for common polymers) places the focal length in the range 9−25 μm for the lenses described in Figures 2 and 3. Interestingly, the numerical aperture (NA) of these lenses should be independent of their size. This is so because

$$\text{NA} = n\sin\phi = n\frac{D}{2f} = n(n_{\text{lens}} - 1)\sin\alpha \qquad (3)$$

Here we used the relationship set by eq 2 and the definition of the numerical aperture, with the symbols defined in Figure 1c. Thus, the numerical aperture is determined solely by the contact angle, which is determined by the liquid−surface combination, is constant for a given set, and does not depend on the deposition time. This allows the manufacture of lenses with varying focal lengths and the same NA.

We used two methods to characterize the optical properties of the microlenses.

(i) Bright field microscopy: This is a rough estimation method; however it is easily implemented and yields good average values. The lenses were placed on the stage of a microscope, and a collimated beam of white light was projected on them by positioning the condenser appropriately.

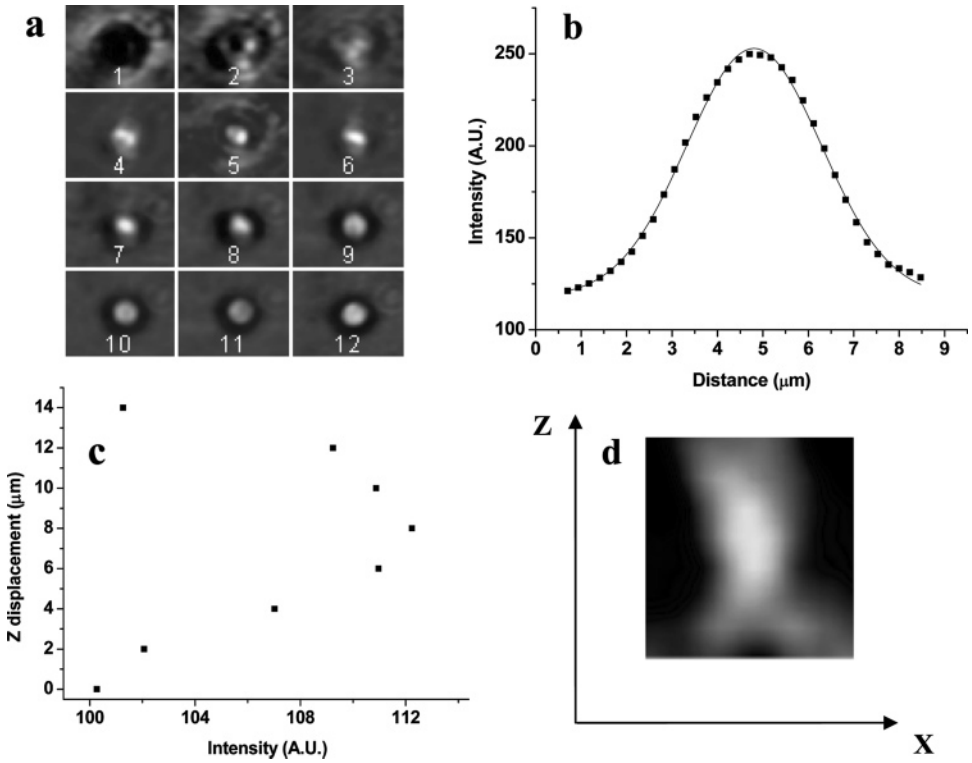

Figure 6. (a) A series of images of the light emanating from the NSOM probe, projected by one microlens onto the APD (see description of setup in Figure 5). The series starts below the plane of the lens (slice 1) through the focal plane (slices 7, 8) and above it (slices 9−14). (b) The intensity profile along the *X* axis (in the focal plane). The continuous line is a fitted Gaussian with a full width at $1/\sqrt{e}$ maximum of 3.0 μm; however it is stressed that this number does not represent the width of the focal point (see text). (c) The intensity profile along the *Z* axis (optical axis of the lens). (d) A stack formed of the slices 1−12 (in Figure 6a) was sectioned along the *X*−*Z* plane, to obtain the light intensity distribution in this plane.

Then images of the lenses were taken at varying planes, through the focal plane. A series of such acquired images is shown in Figure 4a. The series of images labeled 1 through 20 in Figure 4a show the light focused by a single lens, where slice number 1 was taken in the plane below the lens (between the light source and the lens), where the lens acts as a scatterer, and slice number 20 is above the lens' focal plane. A movie is provided as Supporting Information. It can be seen that the focal plane of the lens is reached in slice 14 or 15. The spacing between slices was roughly 2.5 μm; therefore the focal plane of this specific lens is roughly 35 μm above the plane of slice 1, which is approximately 5 μm below the plane of the lens. This corresponds to a focal length of $\sim$30 μm. The stack formed of slices 1 through 20 was sectioned (Figure 4d), to obtain the intensity distribution in the $Z-X$ plane. The intensity profile along the Z axis is plotted in Figure 4c (the horizontal dashed line represents the plane of the lens) and the intensity profile along the X axis is plotted in Figure 4b. The continuous line in Figure 4b is a fit to a Gaussian with a full width at $1/\sqrt{e}$ of its maximum of 3.7 μm, representing the width of the focal spot.

(ii) A more precise method we have used employed a near-field scanning optical microscope (NSOM) probe as a point source of light in *far field*. The lenses were placed on the NSOM scanner; light from the point source was passed through the lenses and was collected in transmission by an avalanche photodiode detector (APD). As the lens was scanned in front of the point source, the image it produced was scanned across the APD, thus measuring the light intensity as a function of X and Y coordinates. The procedure was repeated after changing the Z position of the APD, thus obtaining a stack of images describing the $X-Y$ intensity distribution at various Z positions, or the point-spread function (PSF) of the lens. We stress the fact that the optical resolution of these images is diffraction limited. The NSOM probe served as a point source of light but was positioned in the far field of the lens. A schematic drawing of the measurement setup is presented in Figure 5.

Figure 6a shows the slices numbered 1 through 12, obtained using this measurement method, with slice number 1 taken in a plane below the lens (between the lens and the NSOM probe), where it scatters light, and slice number 12 is above the focal plane, where the image of the point source diverges. It is visible that the focal plane is reached in slice 7 or 8. The intensity distribution in the $Z-X$ plane was obtained by sectioning the stack and is presented in Figure 6d. The intensity profile along the Z axis can thus be obtained (Figure 6c), showing a depth of field of approximately 7 μm. The intensity profile along the X axis, in the focal plane, is plotted in Figure 6b, and a Gaussian fit to the measured points yields a full width at $1/\sqrt{e}$ maximum of 3.0 μm. Importantly this value does *not* represent the width of the focal point: The distance along the X axis is the displacement of the lens relative to the NSOM probe; however the distance traveled by the image of the point source, at the plane of the APD, differs by a factor M, which is the lens magnification. The advantages of this method of characterization are the superior spatial resolution due to the use of the precise

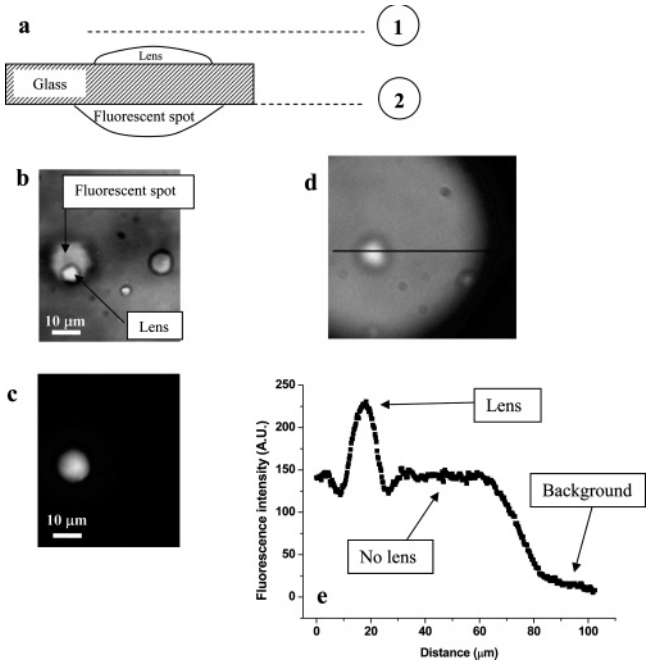

Figure 7. Demonstration of microlens performance in the context of biochips. (a) Schematic representation of the experimental setup: a fluorescent spot and a microlens are deposited on the opposite sides of a coverglass (170 μm thickness) with two different nanopipets. The focal plane of the microlens is labeled **1** and the plane of the fluorescent spot is labeled **2**. (b) A bright-field image of the fluorescent spot and the lens taken in the focal plane of the lens, (**1**). (c) A fluorescence image of the fluorescent spot taken in its plane (**2**). (d) A fluorescence image taken in the focal plane of the lens (**1**). The round halo is the fluorescent light emitted by the fluorescent spot which is out-of-focus (in plane **2**). The bright spot in the center of the halo is the image of the fluorescent spot concentrated by the microlens in its focal plane. (e) An intensity profile along the horizontal line in Figure 7d. The light intensity produced by the microlens is 1.5-fold higher than the light intensity detected directly from the fluorescent spot.

scanner, the use of a genuine point source of light, and the monochromatic light source. For example, more details of the lens can be observed, such as some astigmatism apparent in slice number 6, Figure 6a.

To demonstrate the potential use of such microlenses for nano-biochips, we performed the following experiment. A spot of fluorescein was deposited with NFP on one side of a cover glass (thickness $\sim$170 μm). On the other side of the cover glass, just opposite the fluorescent spot, a microlens was manufactured, with NFP as before. These microlenses have front focal lengths (on the side facing air) in the range of $\sim$30 μm (see Figure 4); since the polymer has a refractive index similar to that of glass, the back focal length (on the side of the glass) is longer by a factor of $n_{glass}/n_{air} = 1.5$, i.e., $\sim$45 μm, therefore the fluorescent spot is at a distance of roughly $4f$ from the lens, and the lens is expected to demagnify the image of the fluorescent spot and concentrate the light it collects. Figure 7a presents a schematic drawing of this setup. Figure 7b is a bright-field image of the fluorescent spot and the microlens, in a plane close to the focal plane of the lens, labeled **1** in Figure 7a. The ability to place the lens precisely over the fluorescent spot of interest is clearly demonstrated here. Figure 7c is a fluorescence

image of the fluorescent spot, taken in the plane of the spot, labeled **2** in Figure 7a. An image of the fluorescent spot was taken through the microlens, in the focal plane of the lens, labeled **1** in Figure 7a, and is shown in Figure 7d. The round halo is the fluorescent light emitted by the fluorescent spot, which is out-of-focus (approximately 200 μm away: 170 μm, the thickness of the coverglass + 30 μm focal length of the lens). The bright area in the middle of the halo is the image of the fluorescent spot projected by the microlens. Evidently, the light intensity in the center of the lens is higher than the light intensity around it. An intensity profile across the center (Figure 7e) shows that a detector placed at this point (in plane **1**, Figure 7a) would have detected 1.5 more light from the fluorescent spot in the presence of the microlens, compared with a scenario without a lens. Obviously, this ratio can be improved by controlling the optical properties of the lens; this should be achievable by tailoring the wetting properties of the polymer/glass combination, deposition time, and refractive index of the polymer.

We presented a method of manufacturing polymer microlenses using NFP. A monomer solution containing a UV initiator is deposited with the nanopipet and subsequently polymerized, to yield microlenses with diameters in the range 4−9 μm. Using this technique, it is possible to place microlenses in strategic locations, with very high positioning precision, and to control their focal length, by varying the deposition time. It was demonstrated that such microlenses can be used to enhance the fluorescent signal from fluorescent sources on the opposite side of a glass support and thus could be very useful in future integrated biochip applications.

Acknowledgment. This work has been partially supported by Grant 346/00 from the Israel Science Foundation and Grant 01-01-01328 from the Israel Ministry of Science, Culture and Sports.

Supporting Information Available: A video showing the printing process of the polymer microlenses and a video showing the light focused by an array of microlenses, as the focal plane is continuously changed. This material is available free of charge via the Internet at http://pubs.acs.org.

References

(1) Danzebrink, R.; Aegerter, M. A. *Thin Solid Films* **2001**, *392*, 223.
(2) Bonaccurso, E.; Butt, H. J.; Hankeln, B.; Niesenhaus, B.; Graf, K. *Appl. Phys. Lett.* **2005**, *86*.
(3) Grunwald, R.; Mischke, H.; Rehak, W. *Appl. Opt.* **1999**, *38*, 4117.
(4) Brenner, K. H.; Kufner, M.; Kufner, S.; Moisel, J.; Muller, A.; Sinzinger, S.; Testorf, M.; Gottert, J.; Mohr, J. *Appl. Opt.* **1993**, *32*, 6464.
(5) Smuk, A. Y.; Lawandy, N. M. *J. Appl. Phys.* **2000**, *87*, 4026.
(6) Liu, G. Y.; Wadu-methrige, K.; Amro, N. A.; Xu, S. *Abstr. Pap. Am. Chem. Soc.* **2000**, *219*, U280.
(7) Kenseth, J. R.; Harnisch, J. A.; Jones, V. W.; Porter, M. D. *Langmuir* **2001**, *17*, 4105.
(8) Wadu-Mesthrige, K.; Amro, N. A.; Garno, J. C.; Xu, S.; Liu, G. Y. *Biophys. J.* **2001**, *80*, 1891.
(9) Wilson, D. L.; Martin, R.; Hong, S.; Cronin-Golomb, M.; Mirkin, C. A.; Kaplan, D. L. *Proc. Natl. Acad. Sci. U.S.A* **2001**, *98*, 13660.
(10) Garno, J. C.; Amro, N. A.; Wadu-Mesthrige, K.; Liu, G. Y. *Langmuir* **2002**, *18*, 8186.
(11) Hyun, J.; Ahn, S. J.; Lee, W. K.; Chilkoti, A.; Zauscher, S. *Nano Lett.* **2002**, *2*, 1203.
(12) Liu, M. Z.; Amro, N. A.; Chow, C. S.; Liu, G. Y. *Nano Lett.* **2002**, *2*, 863.
(13) Ying, L. M.; Bruckbauer, A.; Rothery, A. M.; Korchev, Y. E.; Klenerman, D. *Anal. Chem.* **2002**, *74*, 1380.
(14) Bruckbauer, A.; Ying, L. M.; Rothery, A. M.; Zhou, D. J.; Shevchuk, A. I.; Abell, C.; Korchev, Y. E.; Klenerman, D. *J. Am. Chem. Soc.* **2002**, *124*, 8810.
(15) Agarwal, G.; Naik, R. R.; Stone, M. O. *J. Am. Chem. Soc.* **2003**, *125*, 7408.
(16) Belaubre, P.; Guirardel, M.; Garcia, G.; Pourciel, J. B.; Leberre, V.; Dagkessamanskaia, A.; Trevisiol, E.; Francois, J. M.; Bergaud, C. *Appl. Phys. Lett.* **2003**, *82*, 3122.
(17) Cheung, C. L.; Camarero, J. A.; Woods, B. W.; Lin, T. W.; Johnson, J. E.; De Yoreo, J. J. *J. Am. Chem. Soc.* **2003**, *125*, 6848.
(18) Lee, K. B.; Lim, J. H.; Mirkin, C. A. *J. Am. Chem. Soc.* **2003**, *125*, 5588.
(19) Lim, J. H.; Ginger, D. S.; Lee, K. B.; Heo, J.; Nam, J. M.; Mirkin, C. A. *Angew. Chem., Int. Ed.* **2003**, *42*, 2309.
(20) Renaultt, J. P.; Bernard, A.; Bietsch, A.; Michel, B.; Bosshard, H. R.; Delamarche, E.; Kreiter, M.; Hecht, B.; Wild, U. P. *J. Phys. Chem. B* **2003**, *107*, 703.
(21) Taha, H.; Marks, R. S.; Gheber, L. A.; Rousso, I.; Newman, J.; Sukenik, C.; Lewis, A. *Appl. Phys. Lett.* **2003**, *83*, 1041.
(22) Zieziulewicz, T. J.; Unfricht, D. W.; Hadjout, N.; Lynes, M. A.; Lawrence, D. A. *Toxicol. Sci.* **2003**, *74*, 235.
(23) Bruckbauer, A.; Zhou, D. J.; Kang, D. J.; Korchev, Y. E.; Abell, C.; Klenerman, D. *J. Am. Chem. Soc.* **2004**, *126*, 6508.
(24) Leggett, G. J. *Analyst* **2005**, *130*, 259.
(25) Tabata, H.; Uno, T.; Ohtake, T.; Kawai, T. *J. Photopolym. Sci. Technol.* **2005**, *18*, 519.
(26) Lewis, A.; Kheifetz, Y.; Shambrodt, E.; Radko, A.; Khatchatryan, E.; Sukenik, C. *Appl. Phys. Lett.* **1999**, *75*, 2689.

NL060323E